SCIENCE CHINA
Information Sciences

• **Supplementary File** •

Simultaneous cooperative relative localization and distributed formation control for multiple UAVs

Kexin GUO*, Xiuxian LI & Lihua XIE

School of Electrical and Electronic Engineering, Nanyang Technological University, 639798, *Singapore*

Appendix A Proof of Theorem 0.1

The argument is an adaption of Theorem 2 in [1]. The details are given as follows. Similar to the proof of Theorem 2 in [1], it can be concluded that there exist sufficiently small $\tau, \lambda > 0$ such that

$$\boldsymbol{I} - \boldsymbol{A}_d^\top \boldsymbol{A}_d \geqslant \lambda \boldsymbol{I}, \tag{A1}$$

where $\boldsymbol{A}_d := \boldsymbol{I} + \tau \boldsymbol{A}$. And for any given $\sigma > 0$, there exist η and a closed ball $\bar{\mathcal{B}}_\eta$ contained in $\mathcal{V}$ such that

$$\|b_2(\boldsymbol{\theta}_k, \boldsymbol{\rho}_k)\| \leqslant \sigma, \quad \forall (\boldsymbol{\rho}_k, \boldsymbol{\theta}_k) \in \bar{\mathcal{B}}_\eta. \tag{A2}$$

Construct $V(\boldsymbol{\rho}_k) = \boldsymbol{\rho}_k^\top \boldsymbol{\rho}_k$. By similar argument to (33) in [1], it can be obtained that for $(\boldsymbol{\rho}_k, \boldsymbol{\theta}_k) \in \mathcal{B}_\eta$

$$\begin{aligned}
& V(\boldsymbol{\rho}_{k+1}) - V(\boldsymbol{\rho}_k) \\
=& \boldsymbol{\rho}_k^\top (\boldsymbol{A}_d^\top \boldsymbol{A}_d - \boldsymbol{I}) \boldsymbol{\rho}_k + 2\tau \boldsymbol{\rho}_k^\top \boldsymbol{A}_d^\top P(\boldsymbol{\theta}_k, \boldsymbol{\rho}_k) + \tau^2 \|P(\boldsymbol{\theta}_k, \boldsymbol{\rho}_k)\|^2 \\
& + 2\tau(\boldsymbol{\rho}_k^\top \boldsymbol{A}_d^\top + \tau P^\top(\boldsymbol{\theta}_k, \boldsymbol{\rho}_k))\boldsymbol{w}_k + \tau^2 \|\boldsymbol{w}_k\|^2 \\
\leqslant& -\lambda \boldsymbol{\rho}_k^\top \boldsymbol{\rho}_k + 2\tau \|\boldsymbol{A}_d\| \|b_2(\boldsymbol{\theta}_k, \boldsymbol{\rho}_k)\| \|\boldsymbol{\rho}_k\|^2 \\
& + \tau^2 \|b_2(\boldsymbol{\theta}_k, \boldsymbol{\rho}_k)\|^2 \|\boldsymbol{\rho}_k\|^2 \\
& + 2\tau(\|\boldsymbol{\rho}_k\| \|\boldsymbol{A}_d\| + \tau \|b_2(\boldsymbol{\theta}_k, \boldsymbol{\rho}_k)\| \|\boldsymbol{\rho}_k\|) \|\boldsymbol{w}_k\| + \tau^2 \|\boldsymbol{w}_k\|^2 \\
\leqslant& (-\lambda + 2\sigma + \sigma^2) \|\boldsymbol{\rho}_k\|^2 + 2\eta(1+\sigma)\|\boldsymbol{w}_k\| + \|\boldsymbol{w}_k\|^2.
\end{aligned} \tag{A3}$$

By letting σ small enough such that $2\sigma + \sigma^2 < \lambda/2$, it follows from (A3) that

$$\|\boldsymbol{\rho}_k\|^2 \leqslant c^k \|\boldsymbol{\rho}_0\|^2 + a \sum_{i=0}^{k-1} c^i \|\boldsymbol{w}_{k-1-i}\| + \sum_{i=0}^{k-1} c^i \|\boldsymbol{w}_{k-1-i}\|^2, \tag{A4}$$

where $c := 1 - \lambda/2$ and $a := 2\eta(1+\sigma)$.

Suppose that the function b_1 is continuous with the maximal value $\bar{m}$ on $\bar{\mathcal{B}}_\eta, \forall k \in [0, \infty)$, it has

$$\begin{aligned}
\|\Theta(\boldsymbol{\rho}_k, \boldsymbol{\theta}_k)\| =& \|\boldsymbol{\rho}_k\| \|b_1(\boldsymbol{\rho}_k, \boldsymbol{\theta}_k)\| \\
& \leqslant \bar{m} \|\boldsymbol{\rho}_0\| c^{k/2} + \bar{m}\sqrt{a} \sum_{i=0}^{k-1} c^{i/2} \|\boldsymbol{w}_{k-1-i}\|^{1/2} \\
& + \bar{m} \sum_{i=0}^{k-1} c^{i/2} \|\boldsymbol{w}_{k-1-i}\|.
\end{aligned} \tag{A5}$$

Note that $\boldsymbol{w} \in \ell^{1/2}$, thus existing a constant $M > 0$ such that $\sum_{k=0}^\infty \|\boldsymbol{w}_k\|^{1/2} \leqslant M$ and $\sum_{k=0}^\infty \|\boldsymbol{w}_k\| \leqslant M$, together with (A5) leads to

$$\begin{aligned}
\|\boldsymbol{\theta}_k\| \leqslant& \|\boldsymbol{\theta}_0\| + \frac{\tau \bar{m} \|\boldsymbol{\rho}_0\|}{1 - \sqrt{c}} \\
& + \frac{\tau \bar{m} \sqrt{a}}{1 - \sqrt{c}} \sum_{i=0}^\infty \|\boldsymbol{w}_i\|^{1/2} + \frac{\tau \bar{m}}{1 - \sqrt{c}} \sum_{i=0}^\infty \|\boldsymbol{w}_i\|
\end{aligned}$$

* Corresponding author (email: GUOK0005@e.ntu.edu.sg)

$$\leqslant \|\boldsymbol{\theta}_0\| + \frac{\tau\bar{m}\|\boldsymbol{\rho}_0\|}{1-\sqrt{c}} + \frac{\tau\bar{m}M(\sqrt{a}+1)}{1-\sqrt{c}}. \tag{A6}$$

Therefore, it has

$$\begin{aligned}\|(\boldsymbol{\rho}_k, \boldsymbol{\theta}_k)\| &\leqslant \|\boldsymbol{\rho}_k\| + \|\boldsymbol{\theta}_k\| \\ &\leqslant \|\boldsymbol{\rho}_0\| + (\sqrt{a}+1)M \\ &\quad + \|\boldsymbol{\rho}_0\| + \frac{\tau\bar{m}\|\boldsymbol{\rho}_0\|}{1-\sqrt{c}} + \frac{\tau\bar{m}M(\sqrt{a}+1)}{1-\sqrt{c}}.\end{aligned} \tag{A7}$$

Now we shall prove the sequence $(\boldsymbol{\rho}_k, \boldsymbol{\theta}_k)$ stays in $\mathcal{B}_\eta$ for all k and here the contradiction method is adopted. Suppose that there exists a finite K satisfying $(\boldsymbol{\rho}_k, \boldsymbol{\theta}_k) \in \mathcal{B}_\eta, \forall k \in [0, K]$ but the claim fails for $k = K+1$. Specifically, for the initial state $(\boldsymbol{\rho}_0, \boldsymbol{\theta}_0)$ in a ball $\mathcal{B}_{\eta_0}$ with $\eta_0 > 0$, selecting $\eta_0 < \eta$, $\tau > 0$, and $(\boldsymbol{w}_k)|_{k\in\mathbb{N}}$ all sufficiently small such that

$$2\eta_0 + (\sqrt{a}+1)M + \frac{\tau\bar{m}\eta_0}{1-\sqrt{c}} + \frac{\tau\bar{m}M(\sqrt{a}+1)}{1-\sqrt{c}} < \eta. \tag{A8}$$

Then for $k = K+1$, from (A7), we know

$$\begin{aligned}&\|(\boldsymbol{\rho}_{K+1}, \boldsymbol{\theta}_{K+1})\| \leqslant \|\boldsymbol{\rho}_{K+1}\| + \|\boldsymbol{\theta}_{K+1}\| \\ \leqslant& 2\eta_0 + (\sqrt{a}+1)M + \frac{\tau\bar{m}\eta_0}{1-\sqrt{c}} + \frac{\tau\bar{m}M(\sqrt{a}+1)}{1-\sqrt{c}} < \eta,\end{aligned} \tag{A9}$$

which reveals that $(\boldsymbol{\rho}_{K+1}, \boldsymbol{\theta}_{K+1}) \in \mathcal{B}_\eta$. This contradicts the preceding condition. Hence the claimed result is achieved and the proof is completed.

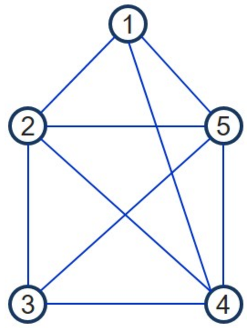

Figure B1 Formation shape and sensing graph for five UAVs.

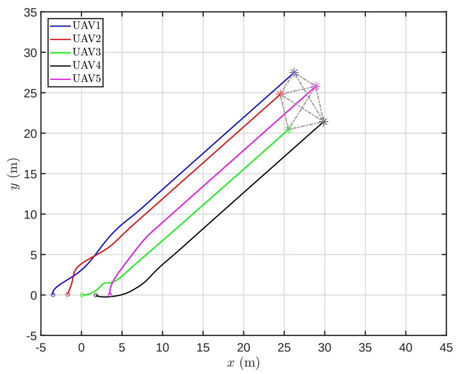

Figure B2 The flight trajectories of 5 UAVs using true RL in noise-free case

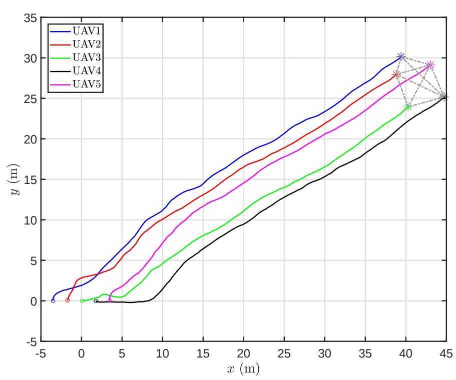

Figure B3 The flight trajectories of 5 UAVs using true RL in noise-contaminated case

Appendix B Figures

References

1 Jiang B, Deghat M, Anderson B D O. Simultaneous velocity and position estimation via distance-only measurements with application to multi-agent system control. IEEE Trans Autom Control, 2017, 62(2): 869-875

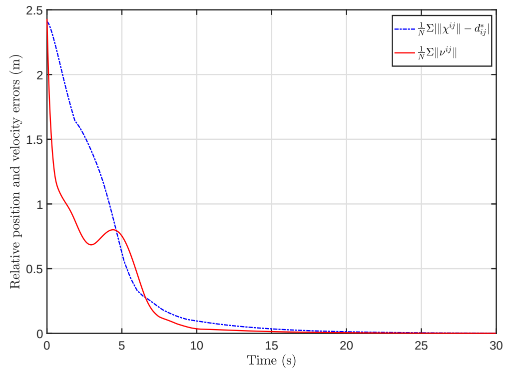

Figure B4 The evolutions of inter-UAV relative velocities and formation shape errors in noise-free case

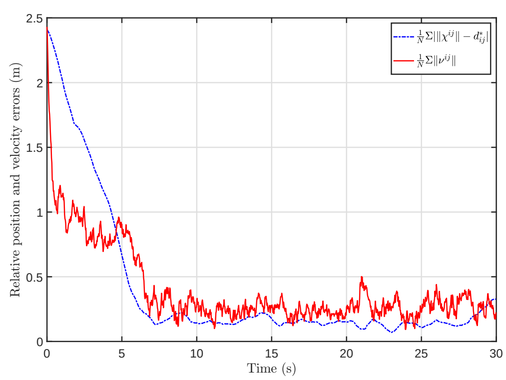

Figure B5 The evolutions of inter-UAV relative velocities and formation shape errors in noise-contaminated case